



ASME Accepted Manuscript Repository

Institutional Repository Cover Sheet

Sebastien

Wylie

First

Last

ASME Paper Tit Reduction in Flow Parameter Resulting from Volcanic Ash Deposition in

Engine Representative Cooling Passages

Authors: Sebastien Wylie, Alexander Bucknell, Peter Forsyth, Matthew McGilvray, David RH Gillespie

ASME Journal Title: Journal of Turbomachinery

Volume/Issue forthcoming

Date of Publication (VOR* Online) 11/10/2016

ASME Digital Collection URL: <http://turbomachinery.asmedigitalcollection.asme.org/article.aspx?articleid=2569438>

DOI: 10.1115/1.4034939

*VOR (version of record)

GT2016-57296

REDUCTION IN FLOW PARAMETER RESULTING FROM VOLCANIC ASH DEPOSITION IN ENGINE REPRESENTATIVE COOLING PASSAGES

Sebastien Wylie*

University of Oxford

Oxford, UK

sebastien.wylie@eng.ox.ac.uk

Alexander Bucknell

University of Oxford

Oxford, UK

Peter Forsyth

University of Oxford

Oxford, UK

Matthew McGilvray

University of Oxford

Oxford, UK

David R. H. Gillespie

University of Oxford

Oxford, UK

ABSTRACT

Internal cooling passages of turbine blades have long been at risk to blockage through the deposition of sand and dust during fleet service life. The ingestion of high volumes of volcanic ash therefore poses a real risk to engine operability. An additional difficulty is that the cooling system is frequently impossible to inspect in order to assess the level of deposition. This paper reports results from experiments carried out at typical HP turbine blade metal temperatures (1163K to 1293K) and coolant inlet temperatures (800K to 900K) in engine scale models of a turbine cooling passage with film-cooling offtakes. Volcanic ash samples from the 2010 Eyjafjallajökull eruption were used for the majority of the experiments conducted. A further ash sample from the Chaiten eruption allowed the effect of changing ash chemical composition to be investigated. The experimental rig allows the metered delivery of volcanic ash through the coolant system at the start of a test. The key metric indicating blockage is the flow parameter which can be determined over a range of pressure ratios (1.01 – 1.06) before and after each experiment, with visual inspection used to determine the deposition location. Results from the experiments have determined the threshold metal temperature at which blockage occurs for the ash samples available, and characterise the reduction of flow parameter with changing particle size distribution, blade metal temperature, ash sample composition, film-cooling hole configuration and pressure ratio across the holes. There is qualitative evidence that hole geometry can be manipulated to decrease the likelihood of blockage. A discrete phase CFD model implemented in Fluent has allowed the trajectory of the ash particles within the coolant passages to be modelled, and these results are used to help explain the behaviour observed.

INTRODUCTION

Ingestion of atmospheric volcanic ash (VA) has long been recognised to be detrimental to gas turbine engines through a variety of mechanisms [1]. However, the atmospheric and engine conditions at which short or long term damage occurs are poorly understood. Acknowledgement of the issue has been elevated in recent years, most notably due to the eruption of Icelandic volcano Eyjafjallajökull in 2010. Limited understanding of ‘safe’ atmospheric concentrations resulted in the cancellation of over 100,000 commercial flights around Europe, at an estimated cost of £1.52bn. In some cases, operators were hours away from bankruptcy [1]. Engine OEMs and the UK Civil Aviation Authority (CAA) have since published regulations authorising commercial flights in regions of ash concentration lower than 2 mg/m³, with additional time-limited flight in concentrations between 2 mg/m³ and 4 mg/m³ [2]. Further research may enable this limit to be safely raised, with the associated economic benefit.

Aside from the economic motivation, the flight safety risk must also be considered. Events such as the surge and flameout of all four engines on flight BA009 in 1982 [3], although rare, demonstrate that high atmospheric concentrations can result in serious short term damage to *all* engines (unlike failures due to mechanical reliability, which are more likely to be confined to a single engine). Undiagnosed long-term damage to hot-end components could furthermore result in blade damage or release.

As global air traffic rises, it must be expected that encounters with volcanic ash will become more frequent. This is exacerbated by rapid traffic growth in regions such as Asia-Pacific, where volcanic activity is prevalent. In Indonesia alone, there are currently 120 active volcanoes [4].

The most damaging mechanism to the performance of the engine is dependent, in the first instance, on the ash concentration, exposure time and engine temperature. At relatively low engine temperatures – conventionally described by the Turbine Entry Temperature (TET) – the dominant damage mechanism is compressor erosion, with the rate of degradation dependent upon the ash concentration. At higher TETs, high ash concentrations are likely to result in heavy accretion on hot components in the main gas path, namely the high pressure NGV blades. The resulting blockage of the primary gas path and decrease in capacity leads to an increase in exhaust gas temperature, which, combined with the blade damage in the core compressor, may lead to surge.

Lower ash concentrations - if encountered over multiple flight cycles - are more likely to reduce the service life of turbine components. The particular mechanism explored in this paper is the ingress of ash into the secondary air system, resulting in particles being fed into the internal cooling passages of the high pressure turbine stage. Due to demands for increasing cycle efficiency, the engine pressure ratio and TET have continually increased, with a typical value in modern engines towards 2000 K, and coolant temperatures of up to 1000 K. There has not, however, been an equivalent change in the allowable metal temperature of the super nickel alloys used for these components. At such temperatures, ash may accrete in the internal cooling passages, altering the distribution of coolant air within the blade and affecting the external coolant films. Convective heat transfer to the coolant is further impaired by the extra thermal resistance of any accreted ash layer. The resulting temperature hotspots have a significant effect on the service life of the component, with the life due to creep being approximately halved for a 15 K increase in metal temperature, increasing the through-life cost of the engine [5].

Hence, there are clear motivations for understanding the key parameters that determine ash accretion, and furthermore, for using design to reduce the susceptibility of internal cooling passages to blockage.

OBJECTIVES

The primary objective of this paper is to identify and quantify factors that cause volcanic ash to deposit within turbine blade internal cooling passages. An experimental test rig was built to study an idealised HP cooling passage with coolant offtake through a series of film-cooling holes. Experimental conditions were varied to investigate the effects of metal temperature, ash particle diameter, dosage, ash source, passage geometry and Reynolds number on the deposition of ash. A complementary CFD study using FLUENT 15.0 simulated the cooling passage continuous flow-field and ingested particle trajectories to allow insight into the features driving deposition.

PREVIOUS WORK INFORMING RESEARCH

Full-Scale Engine Testing

Full scale engine testing in VA conditions has been attempted most recently as part of the Vehicle Integrated

Propulsion Research (VIPR) campaign, which studied ash ingestion into the United Technologies F117 engines of a C-17 aircraft during ground running conditions. Prior to this, Dunn [6] performed analysis on data from full scale engine tests performed at the Industrial Acoustics Engine Cell at Calspan Corporation between 1976 and 1995. A range of particulates were injected, including Mount St Helen's and Twin Mountain black scoria volcanic ash. The results of the Calspan tests confirmed the understanding that deposition is highly dependent upon the ash particle temperature, as this drives particle viscosity (i.e. stickiness). The temperature of the gas at the point of deposition is therefore an important parameter. This being the case, the relevance of both the VIPR and Calspan tests to modern civil large engines and military engines is questionable. All of the engines tested in both campaigns ran with TETs in the range 1200 – 1500 K. This is associated with much lower coolant temperatures, implying that the ash may not heat to as high a temperature during its residence time within the turbine blade: it must therefore be expected that the level of internal deposition behaviour could be different.

Effect of Temperature

The Calspan tests conducted with TETs exceeding 1300 K experienced high deposition on the NGV leading edges and pressure surfaces, and multiple engine surges occurred. Dunn proposed a minimum TET for accretion to occur of 1283 K. Tests conducted at TETs below approximately 1280 K resulted in very minor deposition on hot components, with erosion of compressor aerofoils being the main damage mechanism. Smith [7] performed high temperature ingestion of coal fly ash for engine-scale NGVs. A minimum metal temperature for deposition of approximately 1200K was determined. Furthermore, the measured deposition was significantly greater when no internal coolant air was supplied, implying that blockage of cooling holes is likely to increase the rate of external deposition. Wenglarz et al. [8] and Kim et al. [9] determined that the added thermal resistance due to the accreted ash results in an increased metal temperature, thus further increasing the rate of accretion. The added surface roughness of the accretions results in rapid ash-on-ash deposition. The positive reinforcement of these effects causes a non-linear increase in both accretion rate and metal temperature.

Quantifying Cooling Hole Blockage

Walsh et al. [10] performed experiments on a coupon designed to replicate the showerhead of coolant holes on the leading edge of high pressure turbine blades. Sand and test dust was injected into the internal passages of the coupon, which was held at both room temperature and heated externally to temperatures around 1000°C. The fractional change in a non-dimensional flow parameter (*FP*) was used to quantify the level of cooling hole blockage due to sand accretion. *FP* is defined in Equation 1.

$$FP = \frac{\dot{m} \sqrt{RT_0C}}{P_{0C} \phi_C^2} \quad (1)$$

This quantity may be obtained through manipulation of isentropic compressible gas laws and the ideal gas law, such that it is solely a function of Mach number and fluid properties. It may also be seen as a ratio of momentum force to pressure force for the coolant flow. As blockage of cooling holes increases, for the same coolant supply pressure (and hence pressure ratio) the coolant mass flow decreases. Therefore, a lower FP is measured post-ingestion compared to pre-ingestion for the same pressure ratio. Conducting tests before and after ingestion allows the reduction in flow parameter (RFP) to be calculated. The RFP is defined in Equation 2, where FP_0 is the pre-ingestion value (at the same measurement temperature as FP).

$$RFP = \frac{FP_0 - FP}{FP_0} \quad (2)$$

Substituting for Equation 1, this may be expressed as given in Equation 3.

$$RFP = 1 - \frac{\frac{\dot{m}\sqrt{T_c}}{P_c}}{\frac{\dot{m}_0\sqrt{T_{0c}}}{P_{0c}}}, \quad (3)$$

which notably is independent of ϕ_c .

In the experiments of Walsh et al., metal and coolant temperatures were varied in isolation to demonstrate the effect of each. In a particular test, 0.5 g of ISO Fine test dust was injected, whilst the metal temperature was raised. The RFP increased from around 2 % at room temperature to around 6% at 1000°C. This was followed by a spike to over 10% as the metal temperature rose to around 1080°C. This was attributed to the melting of previously adhered and incoming ash particles. There is therefore a clear dependency of deposition on temperature. Quantifying this using the RFP method for real volcanic ash samples (rather than sand or dust) is a focus of this work.

Effect of Geometry

The results above indicate that the temperature at which rapid deposition occurs is likely to be below modern TETs [5], designing internal passages that are not conducive to particle impact is important. Tu et al. [11] studied the rate of wall impaction and rebound angle for particles in flow over a curved surface. It was concluded that impaction rate was strongly dependent on particle Stokes number, with highly ballistic particles ($St \gg 1$) experiencing both a high impact rate and high restitution, resulting in shallow rebound angles. Both of these effects would increase deposition rate. Jensen et al. [12] performed experiments using ceramic particles where external deposition surfaces were varied in angle between 30° and 90° relative to the mainstream flow. It was observed that deposition thicknesses were up to 20% lower for the shallowest angles – where the requirement for ballistic particles to be turned by the flow is at its minimum. Kuk et al. [13] showed for a single cooling hole that by tuning the turning angle of film-cooling holes to a momentum ratio parameter it was possible to make the film-cooling hole less susceptible to blockage. Further investigation is required to determine how internal deposition

may generally be reduced through judicious choice of film-cooling geometry.

Ash Composition and physical state

Ash compositions and physical states vary between volcanoes and even within a given eruption. The type of eruption is controlled by characteristics of the erupting magma. These characteristics include its chemistry, crystal content, temperature, dissolved gases, and the interaction that it has with water [14]. The type of eruption can then determine the chemistry, particle size distribution, and physical and chemical components of the volcanic ash [15]. The major constituent in volcanic rocks is silicate, SiO_2 . The wt% of SiO_2 can vary between 40 - 80% [16], depending on the type of eruption. Unlike its crystalline structure, the amorphous nature of silicate glass allows VA to soften, distort and stick as it forms a viscous liquid. This occurs as the VA reaches a molten or semi-molten state at a temperature around $\approx 1200K$ [16], depending on the ash source. Despite being a crucial starting point, the softening temperature can only provide limited information about sticking for this research. Inertial characteristics of impacting particles and adhesive forces between the particle and wall must also be considered, as shown by Dunham et al. [17] in their computational viscosity dependent particle-sticking model.

Volcanic ash particle size

Deposition characteristics can be split into three main transport categories as shown in Fig 1: the turbulent diffusion regime, the eddy diffusion-impaction regime and the inertia impaction regime [18]. In the first two regions, body forces such as thermophoresis dominate over the low inertial forces.

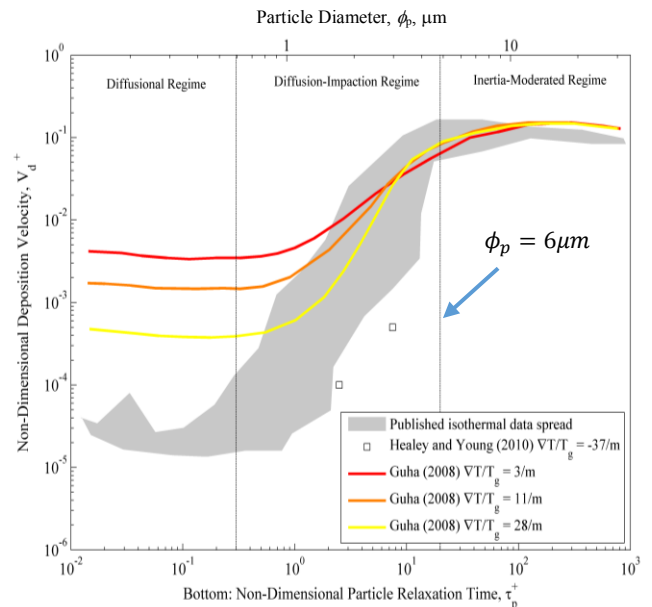


Figure 1: Dimensionless deposition rates vs. dimensionless particle relaxation time and particle diameter (using experimental conditions). Annotated to include the regime change at $\phi_p \approx 6\mu m$ and results from Guha and Healy et al. [18, 19].

Thermophoresis is noteworthy in turbines due to the large temperature gradients that exist, particularly between the blade and coolant gas. However, for larger particles, inertial impaction is particularly important due to the large streamline curvatures required to enter and navigate cooling holes. An elementary analysis using experimental parameters from this research indicates that the transition to the inertial impaction regime takes place at a minimum particle diameter of $\approx 6 \mu m$. This is shown in Appendix A, and also indicated on Fig. 1, where three cases of increasing temperature gradient ($\frac{\nabla T}{T}$) are plotted to show the sensitivity of the deposition velocity. In the current study $\frac{\nabla T}{T} \sim -40$. The closest data available from the literature is that of Healy and Young [19] where $\frac{\nabla T}{T} \sim -37$. Atmospheric VA particles are likely to have diameters above and below this limit at the point of ingestion into the turbine blade.

Particle diameter effects are best described with reference to the Stokes number. This is defined as the ratio of the particle to freestream fluid residence times, as given in Equation 4.

$$St = \frac{\tau_i}{\tau_a} = \frac{\tau_i U_a}{\phi_c} \quad (4)$$

τ_i is the particle relaxation time in non-Stokes flow conditions ($Re > 1$). Equation 5 shows that this is then a function of the

Stokes flow particle residence time ($\tau_p = \frac{\rho_p \phi_p^2}{18\mu_a}$) relative slip Reynolds number (Re_{rel}), drag coefficient (C_d) and Cunningham correction factor ($C_c \approx 1$) [18].

$$\tau_i = \tau_p \frac{24}{Re_{rel} C_d} \frac{C_c}{C_d} \quad (5)$$

When $St \ll 1$, particles will be expected to follow streamlines through regions of rapid change in acceleration and direction. As $St \gg 1$, particles are considered to be ballistic and not easily turned by the fluid flow. Dunham et al [17] used a particle-sticking model in a state of the art combustor to confirm this trend. Experiments conducted by Walsh et al [10] are also in agreement with this, showing that an increase in particle diameter results in a greater amount of deposition.

VA particles of $6 \mu m$ diameter have a Stokes number in the order of 10^0 for experimental conditions used in this research. This demonstrates that the size of particles used in this research is in the lower bounds of ballistic, inertia-driven behaviour. It also suggests that there are multiple possible deposition mechanisms for volcanic ash in internal cooling passages, depending on particle diameter.

Volcanic ash dosage

The VA conditions that have caused engine damage range significantly. The particulate concentration and the engine exposure time both play a pivotal role in deposition, and are the focus of most regulations. This can be quantified using an ash dosage, which is the product of the ash concentration (C_p) and the exposure time (Δt), as shown in Equation 6.

$$D = C_p \Delta t \quad (6)$$

Clarkson et al [20] have placed some key volcanic ash experiments and real-life flight encounters on an exposure vs. ash concentration graph in Fig. 2. It clearly highlights that there is a region of unsafe operation that is dependent on both the ash concentration and the exposure time. However, it is not well understood where the transition between safe and unsafe operation occurs. For example, factors such as the eruption type and engine model (determining TET and passage geometries) would need to be accounted for. The region of the plot associated with long-term damage events – the area of interest of this research – is highlighted, as well as the region associated with in-flight power loss.

The ellipse size of each data point also varies depending on the uncertainty associated with the encounter conditions. There is evidently a need to investigate the effect of the dosage parameter on deposition.

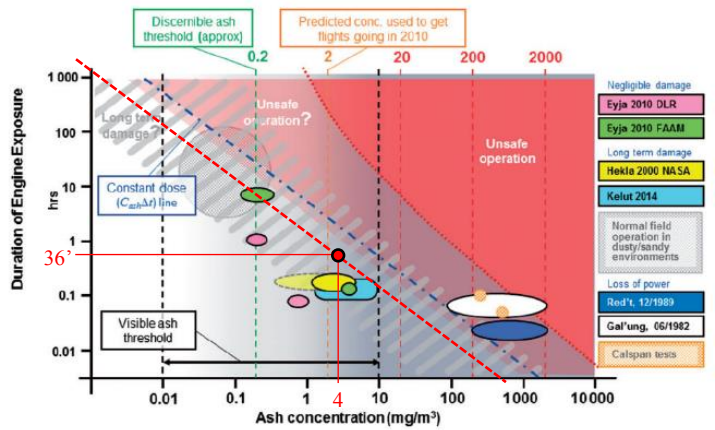


Figure 2: Illustration of known VA encounters, plotted as ash concentration vs exposure time [20]. The experimental dosage line is marked as the red dotted line.

The dosage is tested experimentally by varying the mass of ash ingested. Experimental results conducted by Cardwell et al. [21] and Walsh et al. [10] showed that deposition increases when a greater mass is ingested. However, it is not entirely clear whether their slug-ingestion experimental method jeopardized the one-way coupling assumed throughout. For example, Strömberg et al. [22] showed that one-way coupling is valid only when the particle volume fraction is less than 10^{-4} . As shown in Appendix B, the experiments conducted here satisfy this condition.

Coolant pressure ratio and Reynolds number

The pressure ratio refers to the ratio of the internal coolant supply pressure to the external atmospheric pressure. It affects the deposition by dictating the velocity that the particle-laden flow passes through the cooling passages. An increase in pressure ratio therefore results in a greater driving force across the cooling passages. Walsh et al [10] found that deposition is reduced when the pressure ratio is increased, as particulates are less likely to adhere to the walls. This research aims to reproduce conditions at the leading edge passage of the HP turbine, where a turbulent Reynolds number of order 10^4 can be expected for the coolant

flow [5]. Pressure ratio rather than absolute pressure is typically replicated in deposition research, as pressure ratio, gas-wall temperature ratio and Reynolds number appear critical for driving the ash ingestion.

VOLCANIC ASH CHARACTERIZATION

Two volcanic ash samples were used in this research: from Eyjafjallajökull (Iceland, 2010) and Chaiten (Chile, 2008). The Chaiten sample used in this research is the 0616b bulk ash sample collected for the work conducted by Watt et al. [23]. The original EYJA and Chaiten VA were sampled close to the source, a couple of weeks after each eruption. These are named S5 and S6 respectively. The S5 EYJA sample was sieved to obtain particle sizes as expected in steady state flight. This resulted in progressively larger particle sizes: S1 – S4. The resulting size distributions are quantified using a Malvern Mastersizer 2000, with the Hydro MU attachment for wet dispersion, accurate within 1% [24]. Size distribution results are shown in Fig. 3, with mean diameter values outlined in Table 1. The S2 sample is used for most testing due to the quantity available and its resemblance to particle sizes expected during flight: $\phi_p \approx 10\mu\text{m}$.

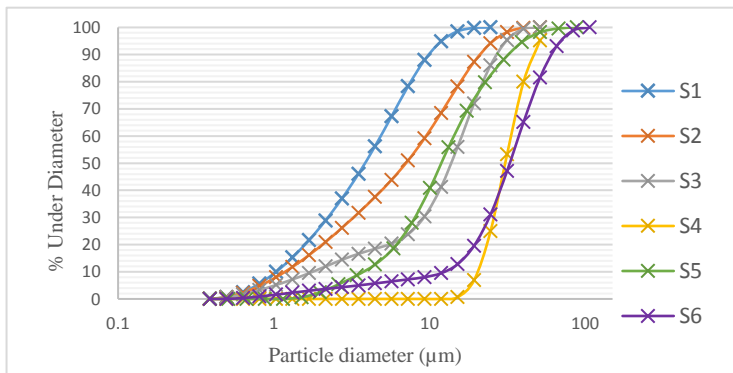


Figure 3: Size distributions for the VA samples S1-S6

Distribution	S1	S2	S3	S4	S5	S6
Mean size ($\bar{\phi}$, μm)	4.79	9.33	14.43	32.24	15.41	34.85

Table 1: VA sample source and mean diameter (all in μm)

A FEI Quanta 650 FEG Scanning Electron Microscope was used to observe the EYJA sample's morphology and to assess its chemical composition. The morphology of the ash is heavily dependent on the formation mechanism. Fig. 4 shows the results for two of the EYJA distributions: S1 and S4. It is clearly seen that the particle shapes are not spherical, but seem to exhibit more of a glass shard-like structure. This is as expected for volcanic ash particles. The particle shape is almost invariant with particle diameter.

Table 2 outlines the chemical composition of some of the main oxides in each volcanic ash sample. A key result to identify is the higher wt % of SiO_2 present in the Chaiten sample. This is as expected from a rhyolitic eruption, compared to the EYJA eruption that contained chambers of both rhyolitic and basaltic

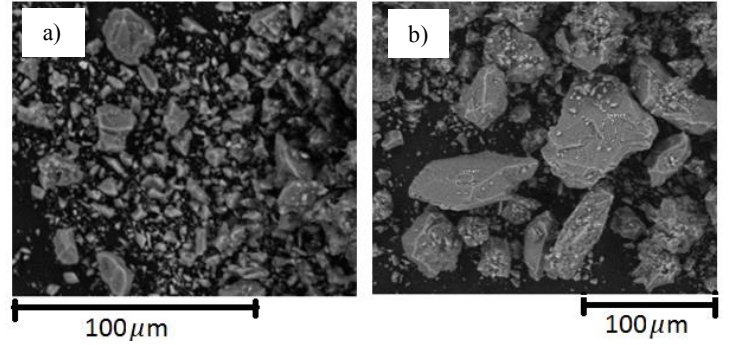


Figure 4: SEM images of EYJA samples S1(a) and S4 (b)

magma. The rhyolite glass found in the Chaiten sample would be expected to have a lower melting temperature than the basaltic ash samples. SiO_2 does not itself indicate the melting temperature of the sample, and while EYJA is seen to sinter at temperatures from $850^\circ\text{C} - 1050^\circ\text{C}$ [15], this behaviour has been seen at a lower temperature for the Chaiten ash [25].

Molecule	Chaiten	EYJA
SiO_2	73.9	51.3
Al_2O_3	14.0	10.9
Fe_2O_3	1.6	9.5
CaO	1.6	4.6
Na_2O	4.1	3.3
K_2O	2.9	2.0
TiO_2	0.2	1.4
Other	1.7	14.7

Table 2: Bulk ash composition (wt %) of the Chaiten sample [23] and the EYJA sample (using SEM)

EXPERIMENTAL FACILITY AND METHODOLOGY

The experimental strategy used in the current study was to preheat an idealised cooling passage test piece to a range of temperatures expected at the metal / TBC boundary in a HP turbine blade. Prior to VA ingestion, the coolant flow to the test section was initiated and the metal temperatures allowed to settle to a steady state condition. Once this was achieved, a fixed mass of volcanic ash (1g) was ingested into the cooling passage, at a concentration of 0.053gm^{-3} . For an engine with an overall pressure ratio of 50, flying through the CAA regulation limit of $C_p = 4\text{mgm}^{-3}$, this mass of ash would be ingested in 36 minutes.

Although the air flow ingested with the VA was unheated, a simple analysis showed that the metal wall temperature only drops by approximately 3 K (< 1%).

Experimental test piece

Three test pieces were designed to model an idealised engine internal cooling passage with film cooling hole offtakes. The test piece typically had three rows of holes with a linear spacing of 2mm between holes, and exhibited 120° rotational symmetry. The main channel diameter (ϕ_c) is 6 mm. The first test piece had 20 film-cooling holes in each row, of diameter $\phi_H = 0.6\text{mm}$,

inclined at 90° to the passage (HD90). The second and third test pieces were orientated in two directions to achieve film-cooling exits at both 45° (HD45) and 135° (HD135) to the incoming flow. For both of these test pieces, the diameter was increased to $\phi_H = 0.75$ mm diameter holes, with 13 holes in each row. The material used for each of the test pieces was grade 304S stainless steel. Fig. 5 shows a sectional sketch of the HD90 test piece. The outer diameter of the test piece is 20 mm and is chosen so that the thermal mass of the test piece is sufficient that it can be considered isothermal throughout the test time.

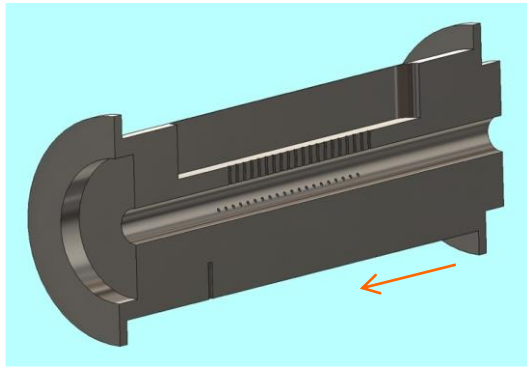


Figure 5: An isometric view of a 180° section through the HD90 test piece using SolidWorks.

Experimental Facility

A schematic of the test rig is shown in Fig. 6. Compressed air enters the facility from a filtered supply and is metered using an Omega 0 – 100 L/min mass flow rate controller. The flow is then split, and a needle valve controls the bypass flow to mainstream mass flow rate ratio. A small fraction of air in the bypass is used to pick up VA in the Continuous Delivery System (CDS). The CDS is able to ingest ash over a longer time when compared to alternative shot/package insertion methods. It therefore allows the dosage rate to be adjusted. The main flow is heated using an in-line heater and 756 W Omega heating tape. It combines with the bypass flow in the mixing chamber, which is then fed through the test piece. The test piece is heated using a well-insulated Wild Barfield 3kW electric kiln. When the coolant

and test piece reach the design conditions, ash is ingested using the CDS to introduce the particle-laden flow.

The total and bypass mass flow rates, and pressure ratio across the test piece are continually monitored, using appropriate pressure transducers and K-type thermocouples. The test piece pressure is measured using a transducer at the entry of the article. Data are captured to a PC using a 16 bit A/D convertor. K-type gas thermocouples measure the temperature of the heated particle-laden flow. Three K-type thermocouples are used to measure the metal temperature of the test piece at depths of 2 mm, 6 mm and 10 mm from the outer surface. The system is controlled from a Labview VI. Whereas the total mass flow rate is reported by the mass flow controller, the bypass flow is metered using a calibrated bespoke orifice meter. Atmospheric pressure is measured whenever the pressure ratio is calculated.

EXPERIMENTAL PROCESSING

The flow parameter vs pressure ratio characteristic of the test piece was measured before and after tests were conducted. From these data the reduction in flow parameter, *RFP*, could be determined. For each sweep of flow parameter, the mass flow controller was used to a set of series of pre-defined mass flow rates and the driving pressure ratio measured. The maximum mass flow rate was limited in each case to ensure that when the *RFP* was measured, the ash deposit was not disturbed. Values required to calculate the flow parameter at each point, such as test piece pressure (P_C) and coolant temperature (T_C), were taken as the average of a large number (> 100) of readings when steady state conditions had been reached. The metal temperatures are the external metal temperature readings taken using the K-type thermocouple inserted at a depth of 2mm from the outer surface.

Fig. 7 illustrates the temporal change in test piece pressure during ash ingestion, when VA: a) doesn't deposit, and b) deposits in the test piece. Fig. 7 a) shows that a transient process exists even when VA doesn't deposit. This could be due to ash bouncing/interacting with the walls, resulting in a temporary hole blockage before particles pass through the system. As shown in Fig. 7 b), the higher steady state pressure reached at the end of the transient ingestion process indicates that the flow

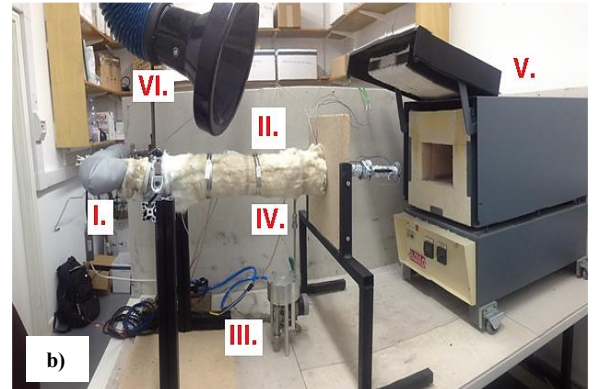
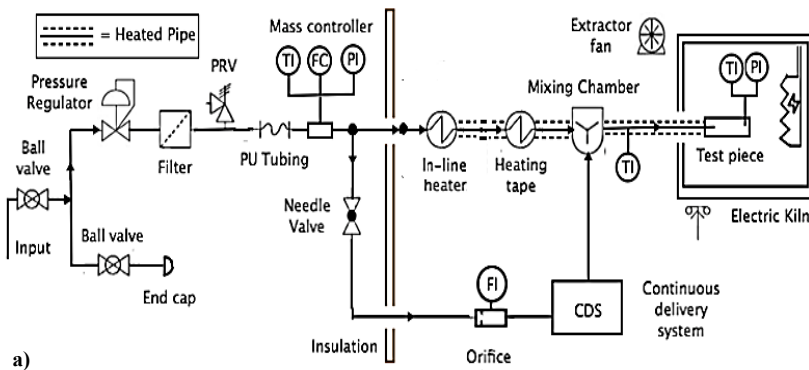


Figure 6: a) Overall process flow diagram b) Hot section of the experimental rig with labelled components: I. = In-line heater, II. = Electric heater tape & insulation, III. = CDS, IV. = Mixing chamber, V. = Electric kiln, VI. = Extractor fan

parameter has decreased and ash has deposited. This results in an increase in the pressure ratio across the cooling passages at a given air mass flow rate. Fig. 8 shows the resulting *FP* for the ingestion of EYJA's S2 sample at $T_m = 1273$ K. To generate the *RFP*, equivalent mass flow rate is required at set pressure ratios and a quadratic fit across the data range is used to do this.

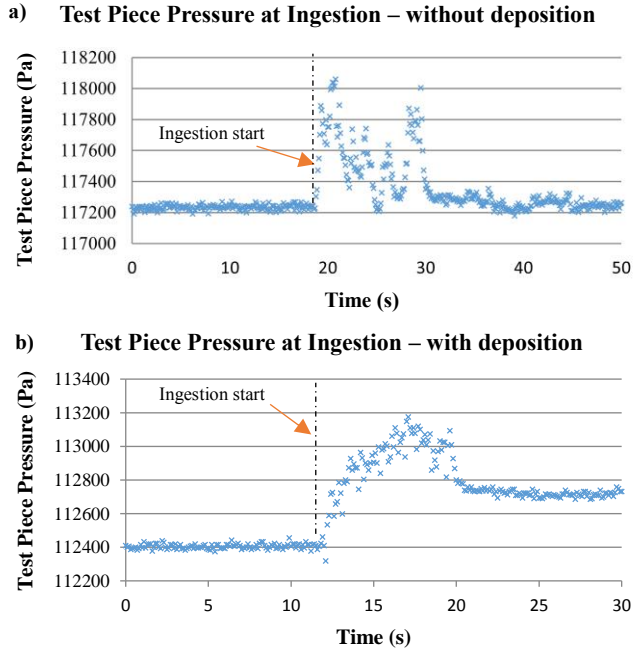


Figure 7: Fluctuation in test piece pressure as ash is ingested into the test piece: a) without deposition, and b) with deposition. The difference in pre-ingestion test piece pressure is due to different experiment metal temperatures.

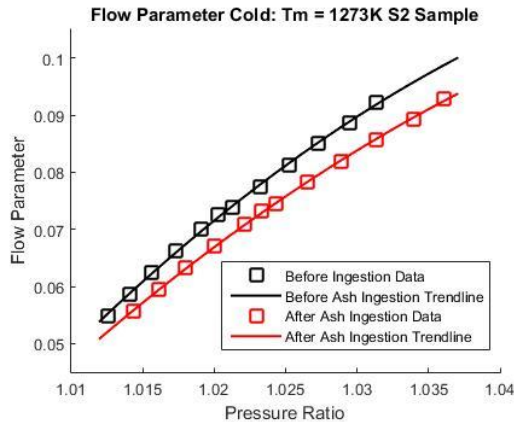


Figure 8: Flow Parameter raw data, and trendline results for the cold calibration of EYJA S2 at $T_m=1273$ K

The *RFP* that was measured at the same pressure ratio as the pre-ingestion condition is marked with a large 'x' in all the results that follow. This can be used to quantify the extent to which particles have deposited at a given test condition. Flow parameters are measured at engine representative coolant temperature, $T_c = 900$ K ('hot') or ambient coolant, 298 K,

('cold'). The geometry is kept constant for each experiment, and so theoretically the pre-ingestion pressure ratio should not change. Unfortunately this was not the case. For the hot characterisation, an increase in the pre-ingestion pressure ratio could potentially be attributed to a potentially slightly different bypass mass flow rate. A likely cause for different pre-ingestion pressure ratios are slight changes in the starting geometry between tests. It is possible that small ash deposits on or within cooling holes were not completely removed when the test piece was cleaned causing a progressive increase in test piece pressure with reuse of the test article.

Negative values of *RFP* are obtained in multiple tests and are assumed to be due to experimental and processing uncertainties. If the cooling holes expanded significantly during heating, this would allow more flow through. For these cases, it was assumed that ash deposition had not occurred, as is confirmed from inspection in Fig. 10 a) for the test where $T_m = 1193$ K.

UNCERTAINTY ANALYSIS

An uncertainty analysis was conducted on the key experimental parameters, using the method of Kline and McClintock [26]. The results are shown in Table 3. The absolute uncertainty in *RFP* value was calculated to be a maximum of 1.74 for a test at 1193 K and pre-ingestion pressure ratio of 1.03. The uncertainty in the cooling hole diameter for either hot or cold conditions is not considered, as it features in the numerator and denominator in the definition of *RFP* (shown in Equation 3).

Parameter	Uncertainty	
	Absolute	Percentage (%)
\dot{m}_a	0.0074 gs^{-1}	0.80
P_a	547 Pa	0.50
T_a	1.00 K	0.11
PR	0.015	1.41
ϕ_p	0.84 μm	1.00
% <i>RFP</i> (RSS error)	1.74	6.32

Table 3: Uncertainty analysis for experimental parameters

EXPERIMENTAL PARAMETERS AND RESULTS

Results are processed and presented as previously discussed. The deposition trends were consistent between RFP_H and RFP_C for all experiments, with the magnitude of $RFP_C > RFP_H$. The RFP_C results are presented for the remaining variables, as the greater reduction in flow parameter magnitudes makes it easier to identify relative amount of deposition.

Metal Temperatures

The electric kiln is used to achieve test metal temperatures ranging from 1163–1293 K. The effect of metal temperature on deposition is investigated and the metal Adherence Threshold Temperature ($T_{m,ATT}$) is located for ingestion of the S2 sample in the HD90 test piece.

RFP_C and RFP_H results are presented in Figure 9. For both sets of results, the reduction in flow parameter is seen to increase

with a rise in metal temperature, as shown in Figure 9 c). This trend is in direct agreement with results found in the literature [6, 10]. While a clear trend is seen in the results, better statistical significance could be achieved by repeating tests. Limited time in the current campaign prevented this. Results therefore clearly show that deposition increases with metal temperature and that the adherence threshold temperature lies in the range: $1208\text{K} < T_{m,ATT} < 1253\text{K}$.

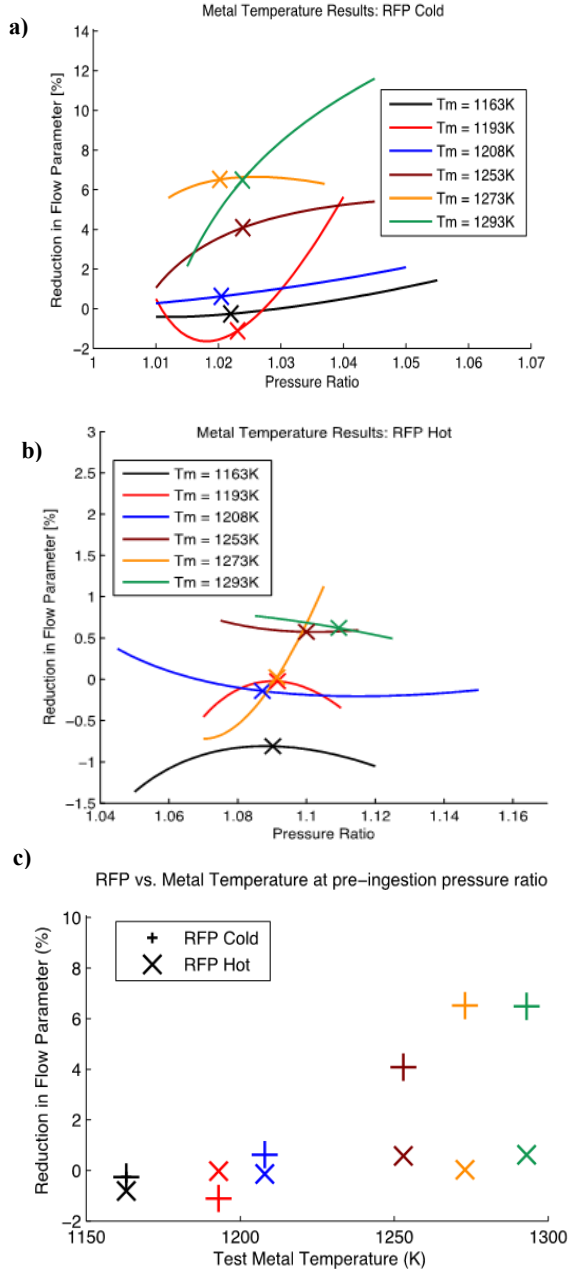


Figure 9: a) RFP_C and b) RFP_H for various metal temperatures c) RFP at the pre-ingestion pressure ratio as a function of metal temperature.

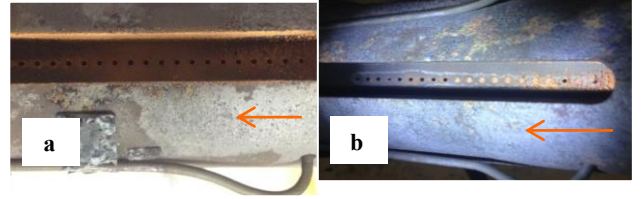


Figure 10: a) Clear passages in the test piece at $T_m = 1193\text{K}$. b) Evidence of deposition in the passages for $T_m = 1253\text{K}$.

Ash Particle Diameters

To investigate the effect of ϕ_p , EYJA samples S1, S3 and S4 were ingested. A metal baseline temperature of $T_{mb} = 1293\text{K}$ is used to test other variables, where $T_{mb} > T_{m,ATT}$. Volcanic ash would always be expected to deposit at this temperature, allowing the relative amounts of deposition to be investigated for other variables.

RFP_C results for each sample are illustrated in Fig. 11. These indicate that deposition tends to increase when larger particle diameters are ingested. This is in direct agreement with experiments conducted by Walsh et al. (albeit, using sand) and CFD simulations completed by Dunham et al. [10, 17].

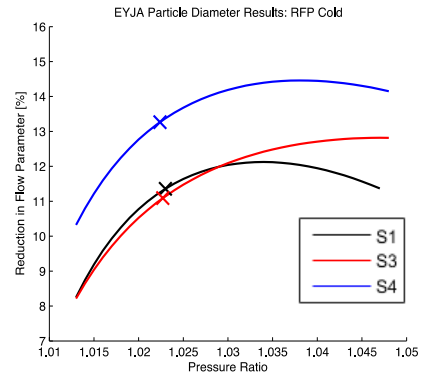


Figure 11: RFP_C results as a function of particle size at $T_m = 1293\text{K}$.

There is noticeably more deposition for the S4 sample than the S1 and S3 samples. Larger particles (i.e. Stokes number $\gg 1$) are unable to follow the streamline curvatures through the cooling holes. Equations 4 and 5 highlight the Stokes numbers' dependency on particle diameters: $St \propto \tau_p \propto \phi_p^2$. It would therefore be expected that $St_{S4} \gg 1$ and that $St_{S4} \gg St_{S3}, St_{S1}$. This results in significantly less deposition for tests conducted using the S1 and S3 samples.

This trend can also be explained when reconsidering the transport regimes detailed in Fig. 1. The turbulent diffusion and eddy diffusion impaction regimes are susceptible to body forces, such as thermophoresis. With the theoretical transition to the inertial impaction regime calculated as $\phi_p \approx 6\mu\text{m}$, body forces may affect deposition for the S1 and S3 samples. Due to the large temperature gradient that exists between the test piece (1293 K) and the coolant flow (900 K), thermophoresis will play a role for smaller particulates. This would result in a further decrease in deposition, as small ash particles approaching the walls impact

with fast moving fluid-phase particles moving down the temperature gradient.

Alternative Materials

The Chaiten (S6) sample is compared against the EYJA (S2) sample. The test is conducted at a lower metal temperature where the EYJA sample showed no deposition. This investigates whether the greater SiO₂ content found in the Chaiten volcanic ash results in a lower ATT to match its lower melting point, when compared to the EYJA volcanic ash.

RFP_C results for each sample are illustrated in Fig. 12. The experiments conducted at $T_m = 1193K$ indicate that the Chaiten volcanic ash deposits below the EYJA sample's empirical ATT range: $1208K < T_{m,ATT} < 1253K$. This highlights the importance of the VA composition and eruption type. It also confirms that the lower melting temperature of the rhyolitic Chaiten sample transfers to a lower ATT. Fig. 13 confirms that extensive deposition occurred for the Chaiten sample test, as a significant number of cooling passages are clearly blocked. It is interesting to note that deposition has occurred in the central passages, whereas the upstream section seems to be relatively clear. This is not in line with most other experimental cases, where deposition was seen to occur initially in the most upstream passages.

Another contributing factor for the deposition seen in the Chaiten sample may be its particle size distribution. As outlined earlier, the sample has a mean particle diameter of $34.9 \mu m$. The particle diameter results for EYJA have just shown that deposition increases with particle size. In fact, the S4 sample has a mean particle size of $32.2 \mu m$, similar to that of Chaiten. Particle diameter results have just shown an increase in RFP_C of $\approx 2\%$ for the S4 sample when compared to baseline sizes (S2).

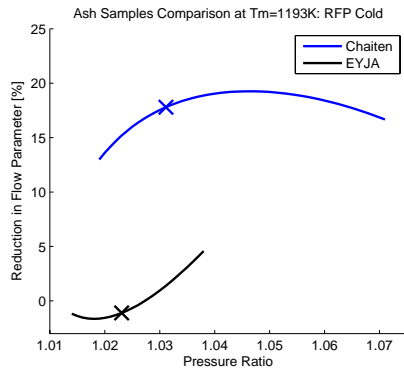


Figure 12: RFP_C for Chaiten and EYJA ash at $T_m = 1193K$



Figure 13: Significant number of passages blocked with the Chaiten ash sample when ingested at $T_m = 1193K$.

Assuming that the effect of particle size is independent of ash composition, the extra deposition due to the Chaiten sample's larger particles would contribute for only a small percentage of the RFP calculated.

Reynolds Number

A Reynolds number of 5000 may typically be reached inside the leading edge cooling hole of a nozzle guide vane (NGV) in a large modern turbofan [5]. The Reynolds number is used to determine the total amount of airflow that passes through the test piece, as shown in Equation 7. Values for the main channel diameter (ϕ_c) and the dynamic viscosity of air at 900 K can then be substituted to give the target mass flow rate of $\dot{m}_a = 0.92 \text{ gs}^{-1}$, as shown in Equation 8.

$$Re = \frac{\rho_a u_a \phi_c}{\mu_a} = \frac{4 \dot{m}_a \phi_c}{\pi \phi_c^2 \mu_a} \quad (7)$$

Therefore:

$$\dot{m}_a = \frac{Re \phi_c \mu_a \pi}{4} \quad (8)$$

The cooling hole Reynolds number will increase during stages of flight where there is a high coolant demand. A case involving a slightly elevated Reynolds number of 7500 is therefore investigated. The required elevated air mass flow rate can be determined using Equation 8. However, to ensure that the dosage is kept constant (see Equation 9 below), the mass of ash ingested must also be increased proportionally. The parameters required to test both Reynolds Number cases are therefore outlined in Table 4. The results are shown in Fig. 14, with the pressure ratio required to achieve the design Reynolds number marked with an 'X'. The Reynolds number does change from this value as the full range of pressure ratios are tested.

Case	Reynolds Number	Air mass flow rate $\dot{m}_a \text{ (gs}^{-1}\text{)}$	Ingested ash mass (g)
Baseline	5000	0.92	1.00
Elevated	7500	1.38	1.50

Table 4: The experimental parameters required for both Reynolds Number experiments

A normalized set of RFP results for the $Re = 7500$ data is plotted in Fig. 14 to account for the different amounts of ash that are ingested into the system. Normalizing in this manner is based on an unproven assumption that the mass of ingested ash is directly proportional to the RFP . Walsh et al. found that RFP was a linear function of the mass of ingested sand for tests conducted at room temperature and at a constant pressure ratio [10]. The results clearly indicate that deposition increases as a function of Reynolds number, even when compared to the normalized set of $Re = 7500$ results. Increasing the mass flow rate by 50% whilst keeping the concentration constant doubled the reduction in flow parameter. One explanation for this is that there would be a greater number of collisions with the test piece walls at a higher Reynolds number where the inertial forces are greater. A counterargument would be that the increase in air mass flow rate

should cause a greater driving force to push ash through the holes, making it more difficult for particles to stick. Evidently the greater number of impactions is more influential here. It should also be noted that the increase in pre-ingestion pressure ratio (shown by the marker "x") can be mostly attributed to the greater driving force that exists as the mass flow rate of air is increased.

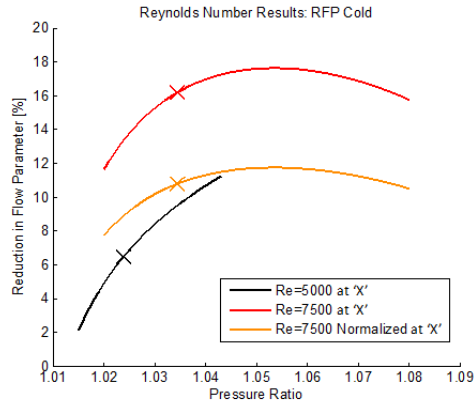


Figure 14: RFP_c as a function of Reynolds number

Dosage

The dosage for this research has been defined as the product of ash concentration and exposure time. The compressor pressure ratio (r_p) in a modern turbofan engine is typically ≈ 50 [5], therefore the concentration of ash in the secondary air system is 50 times greater than the atmospheric concentration, C_p . Equating the volumetric flow rates of air and ash and rearranging yields Equation 9.

$$D = C_p \Delta t = \frac{m_p \rho_a}{\dot{m}_a r_p} \quad (9)$$

To investigate the effect of a rise in dosage, whilst keeping the Reynolds number constant (i.e. $\dot{m}_a = \text{constant}$), only the mass of ash ingested is increased. The dosage for the majority of this research is based on an ingestion of 1g of ash, resulting in a baseline dosage of $D_b = 8.5 \text{ gm}^{-3}\text{s}$. A new CDS plate capable of holding 1.5g of ash was designed and constructed, allowing an elevated dosage of $D_e = 12.8 \text{ gm}^{-3}\text{s}$ to be tested. RFP_c results are shown in Figure 15. Once again, normalized results are processed to account for the increase in the mass of ash ingested into the system. As would be expected, the results indicate that deposition increases with ash dosage. The effect of increasing the concentration of the ash injected by a factor of 1.5 over a given test time period resulted in 3 times the reduction in flow parameter. The non-linear increase in RFP is likely due to the greater number of particle collisions with the test piece wall and the rapid accretion caused by 'ash on ash' deposition. An increase in the number of ash particles ingested per unit time therefore results in more ash deposition within the cooling passages.

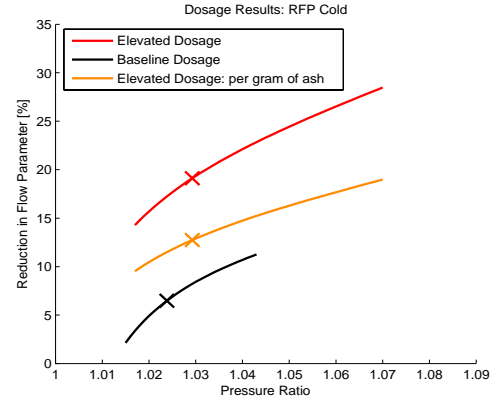


Figure 15: RFP_c as a function of volcanic ash dosage

Effect of Geometry on RFP

Figure 16 shows the reduction in flow parameter (RFP) as a function of pressure ratio for the S5 sample at metal temperatures of 1190 K and 1310 K. Data for two geometries (HD45 and HD135) are presented. Schematics of HD45 and HD135 are shown in Figures 17 a) and b), with accretions sustained in HD45 shown in Figure 18. Previous tests conducted at 1190 K using the S2 particle size distribution did not result in a reduction in the flow parameter. However, the larger mean particle size used in these tests from the S5 sample appears to produce a noticeable RFP .

Figure 16 shows that the peak RFP for HD135 at the 1190 K condition is 9.3 %, 6.5 % greater than the peak RFP for HD45. The difference in peak RFP reduces to approximately 2.7% for the 1310 K condition. The differences in RFP indicate a variation in the deposition patterns between the geometries.

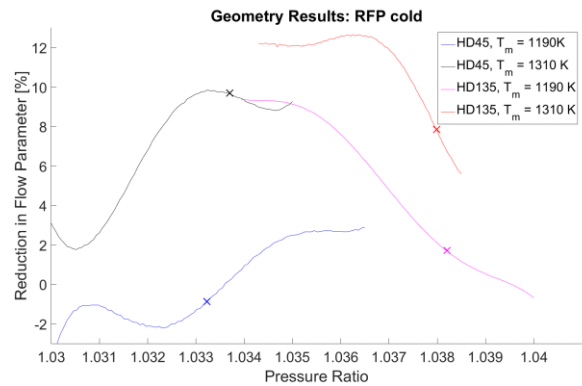


Figure 16: RFP_c vs. PR as a function of test piece geometry and metal temperature

Effect of Geometry on Deposition Location

Figures 18 a) and b) show high levels of deposition inside the four most upstream cooling holes of HD45. The downstream holes were almost entirely clear. The high pressure ratio at the upstream holes leads to a partial turning of the particles (i.e. less than 45°), resulting in impaction on the downstream edge of the cooling hole. As the pressure ratio decreases through the test

piece, the streamwise particle momentum is sufficiently low to allow the particles to escape.

Post-test inspections of HD135 revealed high deposition within the central cooling channel, with wedge-shaped accretions stuck to the downstream rim and first 1-2 mm of the cooling hole. Minimal or no deposition was observed for the remainder of the hole. Extracting and weighing the accreted ash in the central channel and coolant holes demonstrated that approximately 29% of injected ash was deposited in the coolant channels in HD45, compared with 18% in HD135.

The effect of almost all of the cooling holes having a partially blocked inlet area (in HD135), compared to blockage of four of the 20 coolant holes (in HD45) appears to result in a higher *RFP*.

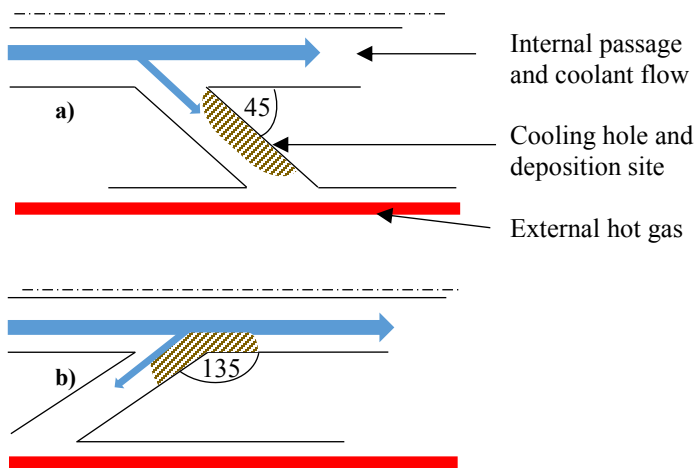


Figure 17: Geometry and main deposition location for a) HD45 and b) HD135

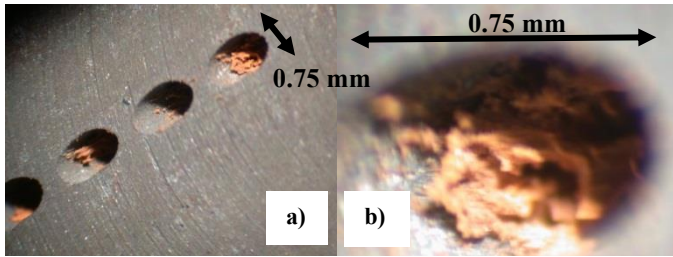


Figure 18 a): Deposition in first four cooling holes of HD45, 1310 K; b) Blocked film cooling hole in HD45, 1310 K

COMPUTATIONAL STUDIES

CFD simulations were run to investigate particle impact location and rates for varying geometries and particle diameters. The results were used to qualitatively explain the overall flowfield and deposition behaviour in the experimental test sections, though are not used in quantitative comparison to the experiments. Development of a robust particle sticking model and use of dynamic meshing is underway to enable this.

ANSYS FLUENT 15.0 was used as the fluid solver and applied the in-built Lagrangian particle model to track the ash particulates. Symmetry of the test pieces allowed the domain to

be reduced to a 60° wedge. Unstructured meshes of approximately 2 million cells were generated using ICEM. 12 prism layers were defined along the cooling channel and hole walls, producing a typical y^+ value of around 6. Doubling the number of cells produced no noticeable change in the flowfield or particle distributions. The $k-\omega$ SST turbulence model was applied, which gives reasonable results for internal flows. It particularly performs better than the $k-\epsilon$ model for pipe flows with sharp offtakes of low length to diameter ratio.

Simulations were run at a nominal case, matched to an experimental external metal temperature of 1293 K. The experimental setup immediately upstream of the test piece – comprising the mixing chamber and pipework – was meshed in order to determine the boundary condition at the inlet of the test piece. The flowfield was characteristic of fully developed turbulent pipe flow, so inlet profiles of temperature and velocity were specified based on a $1/7^{\text{th}}$ power law, with the inlet mass flow rate of coolant matched to that used experimentally. A conjugate heat transfer model was implemented. Figure 19 shows temperature contours for the converged solution. At the far end of the test piece, flow stagnates and temperatures converge towards the metal temperature.

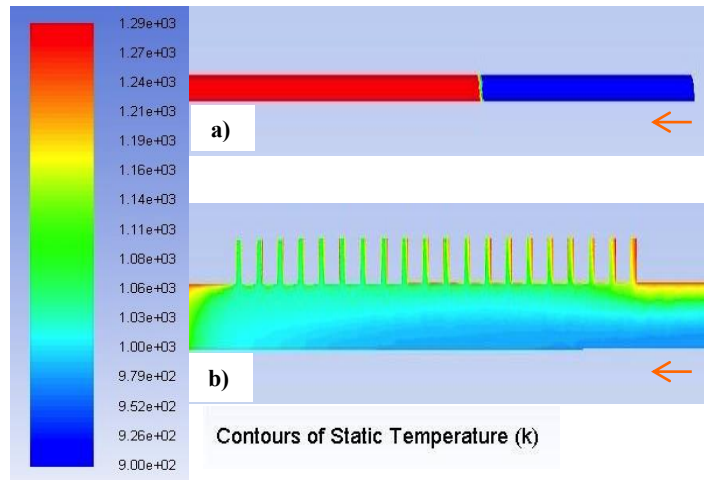


Figure 19: (a) External metal temperature of the feed pipe and test section, showing the defined transition at entry to the kiln (operating at 1293 K). (b) Fluid temperature within the film cooling passage and holes, at the same external temperature.

Particle Trajectory Studies

A trapping wall condition was used on all particle-wall impacts. The number of particles that reached the coolant hole exit - the number 'escaping' - was also recorded.

The particle size distribution of the EYJA ash samples (S1 and S2) were converted into a Rosin-Rammler distribution for use in the simulations. The simulations therefore closely model the particle size distribution encountered in the experiments, and also allow the effect of particle size on trajectory and impingement location to be directly compared.

The Stokes number analysis showed that VA particles of diameter greater than $\sim 6 \mu\text{m}$ are ballistic in nature, implying that their motion is dominated by inertial forces. The trajectories of smaller particles, however, may be influenced by other body forces, and thus these need to be considered for inclusion in the simulation.

A non-spherical particle drag law based on the correlation of Haider and Levenspiel [27] was used. The SEM images suggested a range of polyhedral shapes, with sphericities typically in the range 0.69 - 0.94. An intermediate value of 0.846 was chosen for subsequent simulations.

Particle forces pertinent to two-way coupling (virtual mass and the Basset force) were neglected. Body forces comprising thermophoresis, Saffman's lift force and turbulent dispersion (modelled using a Discrete Random Walk method) were investigated using successive simulations, as shown in Table 5. The smallest injected particles ($3 \mu\text{m}$ diameter) were demonstrably influenced by the thermophoretic force, with approximately 10% more particles able to escape. There was a negligible effect on $10 \mu\text{m}$ and $15 \mu\text{m}$ diameter particles, confirming that inertia-driven deposition is dominant. The results also demonstrate that turbulent dispersion and Saffman's lift force have an almost negligible effect for $3 \mu\text{m}$ particles and no effect for larger particles. These forces were therefore neglected in subsequent simulations. A summary of the parameters used in the particle tracking simulations is given in Table 6.

	% particles trapped		
Particle Diameter (μm)	3	10	15
no additional body forces	81.1	88.4	89.4
thermophoresis implemented	71.6	88.4	89.4
turbulent dispersion implemented	82.2	88.4	89.4
Saffman's lift force implemented	81.7	88.4	89.4

Table 5: Particle trapping rates for selected body forces

ρ_p (kg/m^3)	849	\dot{m}_{ash} (g/s)	0.125
Particle sphericity	0.846	\dot{m}_{air} (g/s)	0.92
ϕ_p (μm)	0-20 (Rosin-Rammler)	$T_{m_{external}}$ (K)	1293
Step length (mm)	0.1	T_p (K)	900

Table 6: Summary of parameters used in particle simulations

Particle Tracking Results

Figure 20 shows particle trajectories, coloured by particle diameter, for the most downstream six cooling holes in HD90. No particles of any size were able to escape in more upstream holes, implying that the high axial momentum of the central channel flow at these upstream positions is not conducive to particles being fully turned through 90° into the coolant holes. This leads to the smallest particles tending to be either deposited on the downstream walls of the first few coolant holes, or escaping in the most downstream coolant holes as shown. $10 \mu\text{m}$ particles are able to escape through the most downstream hole,

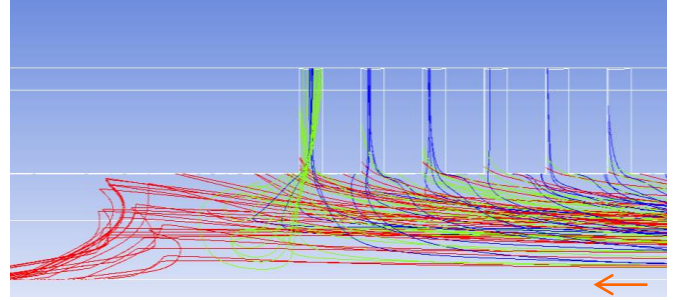


Figure 20: Particle tracks in HD90, showing a cross-section of the test piece at the most downstream 6 holes. Coloured by particle diameter: blue = $3 \mu\text{m}$; green = $10 \mu\text{m}$; red = $15 \mu\text{m}$.

mainly through overshooting it, reaching the stagnation region and then being recirculated into the hole inlet. The $15 \mu\text{m}$ particles are sufficiently ballistic that the maximum angle through which they are diverted is around 45° . This leads to deposition primarily on the central channel wall. The particles that do not deposit continue towards the end of the test piece, where they appear to become entrained in the recirculation region of the bulk flow. This causes particles to descend to the centre of the channel, and finally strike the end wall. This illustrates the importance of a dust hole at the end of blind passages, to allow the largest, most ballistic particles to escape.

Overall, approximately 27% of $3 \mu\text{m}$ particles, 8% of $10 \mu\text{m}$ particles and 2% of $15 \mu\text{m}$ particles were able to escape. Reducing the cooling passage inclination from 90° to 45° resulted in an 8% increase in the number of $3 \mu\text{m}$ particles escaping, but only a 0.1% increase for $10 \mu\text{m}$ and $15 \mu\text{m}$ particles. However, the dominant deposition location in the latter case moved from the central channel to inside the cooling hole walls. This agrees with the experimental findings of blocked upstream holes in HD45. In HD135, the maximum particle turning was $\sim 110^\circ$, resulting in limited deposition inside film cooling holes. Instead, the primary deposition location was on the downstream edges of the hole inlets, and along the full length of the central coolant channel. This agrees with the observed experimental deposition patterns in HD135.

The experimental results suggested that blockage of upstream film coolant holes resulted in a lower *RFP* than blockage along the central channel. However, what is unclear is whether this trend in deposition location is consistent for a longer exposure time or mass loading. To investigate this effect, an additional CFD simulation was run with the first four of the 13 holes in HD45 and HD135 'blocked'. Mass flow of coolant air was kept constant, simulating a constant cooling duty demand. In HD135, around 1% more particles were trapped at this condition, implying the higher suction ratio encountered has little effect on the dominant deposition location. In contrast, the higher suction ratio caused 21.2% more particles to be trapped in HD45, with 18.6% of these being $3 \mu\text{m}$ diameter particles. The flowfield solution indicates that the increased suction ratio has the effect of moving the separation region inside the coolant hole further towards the downstream passage wall. The mainstream

flow overshoots the hole, necessitating a 135° turn to enter the passage inlet. Any 3 µm particles entrained in this mainstream flow will be required to perform the same direction change – resulting in greater deposition inside the coolant passage inlet.

Therefore, for short exposure times, cooling passages inclined at 45° appear to suffer a lower overall *RFP* compared to holes inclined at 135°. However, over longer exposure periods, the blockage of upstream 45° holes can generate flow conditions that are conducive to accretion rate increasing. In contrast, this effect is not observed for 135° holes.

CONCLUSIONS

Volcanic ash depositions inside engine representative cooling passages have been investigated experimentally, with numerical simulations used to give insight into the flow field and particle impact locations. The passage tested has a baseline geometry of 20 cooling holes, at 2.0 mm spacing, and 0.6 mm diameter. The experiments were performed using the following baseline parameters: EYJA ash, coolant temperature of 900 K, metal temperature of 1293 K, passage Reynolds number of 5000, a dosage of 8.5 gm⁻³s and 90° cooling holes. The effect of deposition was quantified by the change in flow parameter and blockage location, the latter through visual inspection. The following observations and conclusions were made when the key parameters were varied:

Metal adherence temperature

- A minimum adherence temperature was inferred from visual observations in the main cooling passage at ~1190 K;
- A change in flow parameter was initially observed at 1208 K to 1253 K.
- The reduction in flow parameter increased with metal temperature up to 6% at a metal temperature of 1293 K; in an engine, this would cause a positive feedback loop as reduced coolant flow causes the metal temperature to increase, thus resulting in further deposition.
- This all points to modern large civil engines being more susceptible to ash deposition as TETs increase.

Volcanic ash type

- Chaiten ash, which has a higher SiO₂ composition, was observed to deposit significantly at a metal temperature of 1193 K (where deposition was not yet present for EYJA ash).
- A reduction in flow parameter of 17% was measured for the Chaiten (S6) sample. This suggests that eruptions from different volcano types could have differing influences on a given engine.

Ash particle diameter

- Larger mean and median sized ash injections caused larger reductions in flow parameter. Numerical simulations of the experiment imply this is due to more inertial driven particulates not being able to follow the streamline out through the cooling holes.

Passage Reynolds number

- Increasing the mass flow rate by 50% whilst keeping the concentration constant doubled the reduction in flow

parameter. A higher coolant flow demand would therefore result in an increase in deposition and hence a reduced cooling effectiveness. For example, this higher demand would be expected at maximum take-off thrust conditions and other transient stages of flight.

Ash Dosage

- Increasing the concentration of the ash ingested by a factor of 1.5 over a given test time period resulted in 3 times the reduction in flow parameter. This suggests that flying through higher concentrations of ash has a non-linear effect on deposition, likely caused by ‘ash on ash’ deposition.

Film cooling hole angle

- Upstream angled holes resulted in 25-50% higher reduction in flow parameter than downstream angled holes. Downstream angled holes were observed to have deposition on the downstream edge inside the coolant holes whilst upstream angled holes experience deposition on the downstream edge of the film cooling hole entrance.
- Increasing dosage results in faster accretion rates in the downstream angled holes, though has limited effect on upstream facing holes.

To conclude, the experimental results presented have highlighted the relative importance of several key parameters. These indicate that the concentration of particles in a given ash cloud is not a standalone criteria to predict engine damage, even if it is the most influential. This research has shown that prediction models must also account for the exposure time, coolant flow demand, type of volcanic ash being ingested and engine model (thus expected TET). Further research is required to understand to what extent an engine is damaged when a given amount of volcanic ash has deposited and the suitability of the current regulation limits.

ACKNOWLEDGMENTS

The authors would like to firstly thank Trevor Godfrey, James Parry Crooke, Sam Hussain, Gerald Walker and Duncan Blake of the Osney Thermofluids Laboratory who helped to develop and maintain the experimental test rig. Secondly, thanks also to Owen Green and Prof. David Pyle, of the Oxford University Department of Earth Sciences, for allowing this research access to equipment and your expertise. Thanks also go to Dr. Rory Clarkson of Rolls-Royce Plc for enthusiasm and support of this work.

NOMENCLATURE

ATT	Adherence Threshold Temperature
C _c	Cunningham correction factor
C _d	Drag coefficient
C _p	Ash concentration
D	Dosage
DPM	Discrete Phase Model
EYJA	Eyjafjallajökull
FP	Flow Parameter
k	Thermal conductivity or erosivity
\dot{m}	Mass flow


NGV	Nozzle Guide Vane
P	Pressure
PR	Pressure ratio
r_p	Compressor pressure ratio
Re	Reynolds number, $= \frac{\rho U D}{\mu}$
RFP	Reduction in Flow Parameter
SEM	Scanning Electron Microscope
St	Stokes number $= \frac{\tau_l}{\tau_a}$
SX	Volcanic ash sample 'X'
T	Temperature
TET	Turbine Entry Temperature
U	Velocity
VA	Volcanic Ash
VIPR	Vehicle Integrated Propulsion Research
wt %	Percentage by weight
y^+	Dimensionless wall distance, $= \frac{u_* y}{\nu}$
u^*	Friction velocity, $= \sqrt{\frac{\tau_w}{\rho}}$

Greek

ρ	density
μ	dynamic viscosity
Φ	volume fraction
ϕ	diameter
τ_l	inertial residence time
τ_p	Stokes flow residence time $= \frac{\rho_p \phi_p^2}{18\mu}$
τ_w	wall shear stress

Subscripts

0	pre-ingestion unblocked parameter at the blocked pressure ratio
a	air parameter
b	baseline test conditions
B	post-ingestion blocked parameter
C	characteristic, coolant, cold (ambient)
D	characteristic length
cr	critical
e	elevated conditions parameter
f	fluid
H	heated conditions
m	metal
m,ATT	metal adherence threshold temperature
p	particle
rel	relative to particle
s	softening

Arrow indicating flow direction 

REFERENCES

- [1] Institute of Mechanical Engineers (IMEchE). 2010. "Volcanic Ash, To Fly or Not to Fly?" *Institute of Mechanical Engineers*. Accessed February 1, 2016. <http://www.imeche.org/docs/default-source/1-oscar/reports->

- policy-statements-and-documents/volcanic-ash---to-fly-or-not-to-fly.pdf?sfvrsn=0.
- [2] Civil Aviation Authority. n.d. *Managing Ash in UK airspace*. Accessed April 27, 2014. <https://www.caa.co.uk/Safety-initiatives-and-resources/Safety-projects/Volcanic-ash/Managing-ash-in-UK-airspace/>.
- [3] BBC. 2010. *When volcanic ash stopped a Jump at 37,000ft*. April 15. Accessed February 1, 2016. <http://news.bbc.co.uk/1/hi/magazine/8622099.stm>.
- [4] Sky. 2015. *Indonesia Raises Volcano Alert Level*. June 3. Accessed February 1, 2016. <http://news.sky.com/story/indonesia-raises-volcano-alert-level-10357196>.
- [5] Ireland, Peter. 2015. "Turbine Internal Cooling." Lecture Series.
- [6] Dunn, MG. 2012. "Operation of Gas Turbine Engines in an Environment Contaminated With Volcanic Ash." *ASME J Turbomach* 051001-051001-18. doi:10.1115/1.4006236.
- [7] Smith, C. S. 2010. "Experimental Validation of a Hot Gas Turbine Particle Deposition Facility." Master's Thesis, Department of Aeronautical and Astronautical Engineering, The Ohio State University.
- [8] Wenglarz, R A, and R G Fox. 1990. "Physical Aspects of Deposition From Coal-Water Fuels Under Gas Turbine Conditions." *ASME J Eng Gas Turb Power* (ASME) 112(1):9-14. doi:10.1115/1.2906484.
- [9] Kim, J., M. G. Dunn, A. J. Baran, D. P. Wade, and E. L. Tremba. 1993. "Deposition of Volcanic Materials in the Hot Sections of Two Gas Turbine Engines." *J Eng Gas Turb Power* 115(3):641-651. doi:10.1115/1.2906754.
- [10] Walsh, W. S., K. A. Thole, and Chris Joe. 2006. "Effects of Sand Ingestion on the Blockage of Film-Cooling Holes." *ASME Turbo Expo 2006: Power for Land, Sea and Air*. Barcelona: ASME.
- [11] Tu, J. Y., G. H. Yeoh, Y. S. Morsi, and W. Yang. 2004. "A Study of Particle Rebounding Characteristics of a Gas-Particle Flow over a Curved Wall Surface." *Aerosol Science and Technology* 38 (7): 739-755.
- [12] Jensen, Jared W., Sean W. Squire, Jeffrey P. Bons, and Thomas H. Fletcher. 2004. "Simulated Land-Based Turbine Deposits Generated in an Accelerated Deposition Facility." *ASME J Turbomach* 127(3):462-470. doi:10.1115/1.1860380.
- [13] Kuk, V. H. M., P. T. V. Jones, and M. G. Rose. 1994. "Particle Deposition in Gas Turbine Blade Film Cooling Holes." *Propulsion and Energetic Panel (PEP)*. Rotterdam: AGARDCP-558.
- [14] U.S. Geological Survey. 2009. *Ash properties & dispersal by wind*. <http://volcanoes.usgs.gov/ash/properties.html>.
- [15] Kueppers, U., C. Simarelli, K. U. Hess, J. Taddeucci, F. Wadsworth, and D. Dingwell. 2014. "The thermal stability of Eyjafjallajökull ash versus turbine ingestion test sands." *Journal of Applied Volcanology*.
- [16] Song, W., K. U. Hess, D. Damby, F. Wadsworth, Y. Lavallee, C. Cimarelli, and D. B. Dingwell. 2014. "Fusion characteristics of volcanic ash relevant to aviation hazards." *Geophysical Research Letters AGU Journal*.

- [17] Dunham, D., J. Carrotte, and M. Zedda. 2011. *Particle trajectories in a state of the art combustor*. Loughborough: NEWAC.
- [18] Guha, A. 2008. "Transport and Deposition of Particles in Turbulent and Laminar Flow." *Annual Review of Fluid Mechanics* 40: 311-341.
- [19] Healy, D. P., and J. B. Young. 2010. "An experimental and theoretical study of particle deposition due to thermophoresis and turbulence in an annular-flow." *Int. J. Multiphase Flow* 870-881.
- [20] Clarkson, R. J., E. J. E. Majewicz, and P. Mack. 2016. "A re-evaluation of the 2010 quantitative understanding of the effects volcanic ash has on gas turbine engines." *Proc. of the IMechE Part G: Journal of Aerospace Engineering*.
- [21] Cardwell, N. D., K. A. Thole, and S. W. Burd. 2010. "Investigation of Sand Blocking Within Impingement and Film-Cooling Holes." *ASME J Turbomach* 021020-021020-10. doi:10.1115/1.3106702.
- [22] Strömberg, T., G. Brethouwer, G. Amberg, and A. V. Johansson. 2012. "Modelling of turbulent gas-particle flows with focus on two-way coupling effects on turbophoresis." *Powder Technology* 224: 36-45.
- [23] Watt, S., D. Pyle, T. Mather, R. Martin, and N. Matthews. 2009. "Fallout and distribution of volcanic ash over Argentina following the May 2008 explosive eruption of Chaiten, Chile." *Journal of Geophysical Research*.
- [24] Malvern. n.d. *Mastersizer 2000 - Support*. Accessed January 20, 2015. <http://www.malvern.com/en/support/product-support/mastersizer-range/mastersizer-2000/>.
- [25] Castro, J. M., and D. B. Dingwell. 2009. "Rapid ascent of rhyolitic magma at Chaiten volcano, Chile." *Nature* 461: 780-783.
- [26] Kline, S. J., and F. A. McClintock. 1953. "Describing Uncertainties in Single-Sample Experiments." *Mech. Eng.* 3.
- [27] Haider, A., and O. Levenspiel. 1989. "Drag Coefficient and Terminal Velocity of Spherical and Nonspherical Particles." *Powder Technology* 58: 63-70.

APPENDIX A

Calculation of Particle Diameter at Inertial Deposition Regime

The particle diameter at the transition point between the inertial and eddy impaction deposition regimes may be determined by calculating the dimensionless particle relaxation time, as given by Guha [18] and reproduced in Equation A1.

$$\tau_{p+} = \frac{\rho \tau_l u_*^2}{\mu} \quad (A1)$$

Where τ_l and u_* are as defined in the nomenclature. The wall shear stress is calculated using

$$\tau_w = f \frac{1}{2} \rho_a \overline{U_\infty}^2 \quad (A2)$$

The Blasius relation for the friction coefficient in smooth pipes is utilised, given by

$$f = 0.079 Re^{-0.25} \quad (A3)$$

For a representative geometry at the experimental mass flows and high temperature conditions, a 6 μm particle has a τ_{p+} of approximately 40. From Figure 1, this value of τ_{p+} confirms that particles of approximately 6 μm diameter are at the transition point to the inertia-driven deposition regime. The experimental values (at $T = 900\text{ K}$) are shown in Table 6.

APPENDIX B

Calculation of Particle Volume Fraction

The particle volume fraction is calculated as shown in Equation B1.

$$\Phi_p = \frac{\dot{V}_p}{\dot{V}_p + \dot{V}_a} = \frac{\frac{\dot{m}_p}{\rho_p}}{\frac{\dot{m}_p}{\rho_p} + \frac{\dot{m}_a}{\rho_a}} \quad (B1)$$

Substituting values for mass flow rates and densities, given in Table 7, yields a volumetric fraction of 6.26×10^{-5} . This satisfies the condition for one-way coupling, as given by Strömberg et al. [22].

$\rho_p = 849\text{kgm}^{-3}$	$\rho_a = 0.391\text{kgm}^{-3}$	$Re = 5000$
$\dot{m}_a = 0.92\text{gs}^{-1}$	$\mu_a = 3.897 \times 10^{-5}\text{Pas}$	$\phi_c = 6\text{mm}$
$\dot{m}_p = 0.125\text{gs}^{-1}$		

Table 7: Experimental values used for calculations in Appendix A and B.